Investigation of Injectant Molecular Weight and Shock Impingement Effects on Transverse Injection Mixing in Supersonic Flow

Scott Kuhlman Burger

Thesis submitted to the faculty of the Virginia Polytechnic Institute and State University in partial fulfillment of the requirements for the degree of

Master of Science

In

Aerospace Engineering

Joseph A. Schetz, Chair

William J. Devenport

Kevin B. Kochersberger

April 13th 2010

Blacksburg Virginia

Keywords: scramjet, injection, mixing, molecular weight

Investigation of Injectant Molecular Weight and Shock Impingement Effects on Transverse Injection Mixing in Supersonic Flow

Scott K Burger

ABSTRACT

This study examines the effect of varying injectant molecular weight on the penetration of transverse injection jets into a supersonic crossflow. The injectants considered here are methane (W=16.04), air (W=28.97) and carbon dioxide, (W=44.01). These results augment the previous results obtained at Virginia Tech for helium (W=4.00) injection under the same test conditions to provide a very wide range of molecular weights. Second, since shocks are ubiquitous in scramjet combustors, their influence on penetration and mixing was also studied by arranging for an oblique shock to impinge near the injection station. The cases of a shock impinging upstream and downstream of the injector were both examined. One can anticipate an important influence of molecular weight here also because of the importance of density gradients on the generation of vorticity by baroclinic torque. Increasing molecular weight was found to increase penetration in general, as well as increase the lateral spreading of the plume. The majority of the data shows a weak dependency of the jet size on molecular weight, but there are indications that under certain circumstances large changes in the flow structure may occur due to molecular weight effects. The addition of an impinging shock is found to increase mixing and decrease penetration and plume size, especially with the shock impinging downstream of the injector.

ACKNOWLEDGEMENTS

I would like to acknowledge the help I received from current and past students of the Virginia Tech research group, especially Ryan Throckmorton, Chris Rock, and Luca Maddalena.

I would also like to acknowledge my advisor, Dr. Joseph Schetz, whose advice and encouragement were invaluable to me throughout the course of my studies.

Lastly, and most importantly, I would like to thank my parents for their unflagging support, without which none of this would have been possible.

photographs by Scott Burger

TABLE OF CONTENTS

LIST OF FIGURES

LIST OF TABLES

NOMENCLATURE

A_j = injector area

A^* = choked throat area

A_c = sensor plane area

C_d = discharge coefficient

C^* = Characteristic velocity

d_j = jet diameter

d_{eff} = effective diameter

f = stoichiometric fuel-air ratio

I_f = hot film electrical current

k = thermal conductivity

l = hot wire sensing length

M = Mach number

M_* = Mach number defect

$\dot{m}$ = mass flow rate

p = pressure

p_c = cone-static pressure

$p_{t,Pitot}$ = Pitot pressure

q = dynamic pressure

$\overline{q}$ = jet-to-free-stream momentum flux ratio

Q_f = hot film heat transfer

$\mathbb{R}$ = universal gas constant

R = electrical resistance

T = temperature

t = time

u = flow velocity

V = voltage

$\mathbb{V}_y\left(d_{eff}\right)$ = vortex center height

$\mathbb{V}_z\left(d_{eff}\right)$ = horizontal center vortex spacing

W = injectant molecular weight

X = axial distance downstream of injector center

Y = lateral distance from the injector centerline

Z = vertical distance from the wall

$\bar{z}_{M_*}$ = vertical location of Mach number defect centroid

$y^{\pm}$ = plume width

z^{+} = plume core height

α = Mass fraction

γ = ratio of specific heats

ρ = density

θ = pitch angle

Γ = circulation

φ = roll angle

Subscripts

j = jet-exit property

t = total condition

f = hot film

∞ = free-stream property

I. INTRODUCTION

For many decades rockets have provided the only means of propelling a vehicle to hypersonic speeds. While rockets have proven themselves a useful and robust form of propulsion their need to carry their own oxidizer is a huge drawback for atmospheric flight where the ambient air could be used for the same purpose. If the weight of the oxidizer could be removed then a much larger payload could be carried or a much smaller vehicle be employed; thus for nearly as long as rockets have been in use research into air breathing hypersonic propulsion has been pursued.

Collecting air while traveling at supersonic speeds for use in combustion is extremely difficult. The high Mach number makes any mechanical compressor unnecessary and impractical due to the high stagnation temperature and pressure. In fact even slowing the incoming air by ram pressure alone to subsonic speeds creates unacceptably high temperatures, so the flow must remain supersonic throughout the entire engine. An engine that operates in this manner is called a supersonic combustion ramjet (scramjet). A diagram of this type of propulsion system is shown in figure 1. The incoming air is compressed by a series of shock waves created by the vehicle forebody and inlet cowling, fuel is injected into the still supersonic air flow and combustion occurs. The combustion products are then accelerated by a nozzle to produce thrust.

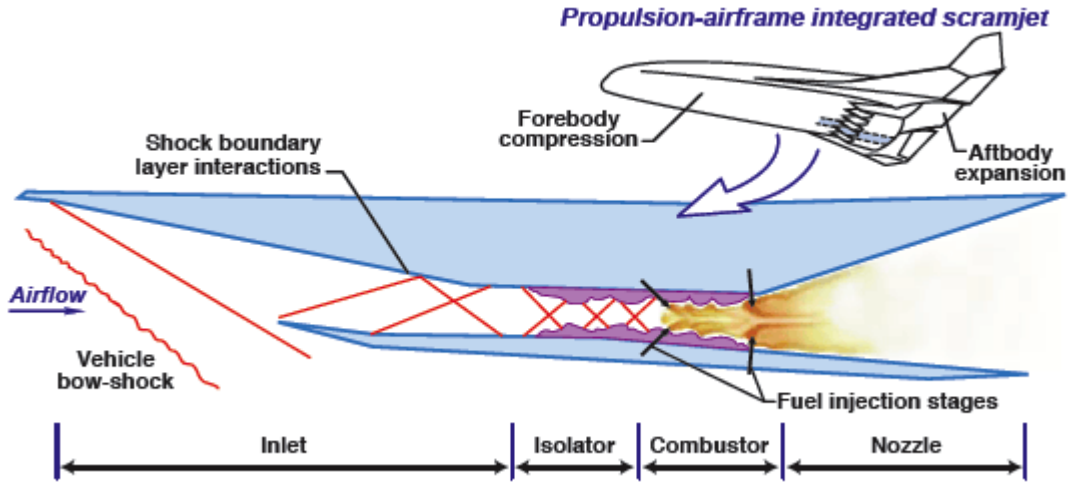

Figure 1. Diagram of a scramjet [www.nasa.gov/centers/langley]

Because scramjet propulsion relies on ram pressure it will not operate at lower flight speeds and must be combined with a secondary propulsion system to boost the vehicle to supersonic flight speeds. In experimental vehicles this secondary propulsion has been provided by rocket motors, but in more advanced design called a Turbine Based Combined Cycle (TBCC) a turbojet in parallel with the scramjet flow path could provide the starting thrust. This design offers the promise of much greater flexibility of operation.

In the near term a vehicle of this type could potentially be used by the military as a rapid response cruise missile or reconnaissance platform. In a more advanced form a scramjet powered aircraft could be used for high speed transport or as part of a space access system.

Research on scramjet propulsion has been ongoing with cyclical levels of interest in funding since the early 1960s. Curran[1] gives an overview of this history and Fry[2] gives a broader overview of scramjet propulsion in the framework of high speed ramjet propulsion since before the Second World War.

The most notable early pioneer in scramjet development was Antonio Ferri who, remarkably, was working on a three dimensional scramjet engine with wide Mach number operability range as early as 1961. This project was called the low-speed fixed-geometry scramjet, and was researched at the General Applied Science Laboratories with funding from the U.S. air force.

Much of the research inspired by this early work focused on axis-symmetric designs. In the U.S. the NASA Hypersonic Research Engine (HRE) was designed to fly as an auxiliary powerplant on the hypersonic, rocket-powered, X-15 but was unfortunately limited to ground tests due to the cancellation of the X-15 program in 1968. A conceptually similar program was pursued in France called ESOPE. This was also planned for flight tests but due to budget constraints were scaled back to two series of ground tests in 1970 and 1972.

Funding for scramjets waned throughout the 1970s and early 1980s. Interest in scramjets was resurrected with the National Aerospace plane (NASP) program, which had the goal of creating a single stage to orbit (SSTO) vehicle which would accelerate under scramjet power from Mach 4 to 15. A great deal of research into engine-airframe integration was done under the auspices of this program and a great deal of test data was obtained. While the program was eventually cancelled two less ambitious offshoot programs emerged. These were NASA's Hyper-X and the U.S. air force HyTech.

In 2004 the X-43A and experimental aircraft built as part of the NASA hyper-X program, succeeded in becoming the first aircraft to achieve sustained acceleration under scramjet power. It eventually demonstrated a top speed of Mach 9.6. This will be followed up in the very near future by the HyTech program's X-51A which will, if successful, maintain scramjet operation for several minutes, much longer than the X-43. The X-51A will also demonstrate, for the first time in a scramjet flight test, the use of fuel to actively cool its high temperature surfaces.

Scramjet engines are generally characterized by extremely small flow residence times in the engine. This short residence time of the flow particularly handicaps the fuel/air mixing process, which needs to be enhanced significantly if the fuel is to be mixed thoroughly with the incoming air. Increasing the effectiveness of the mixing process allows for a shorter combustor, reducing weight and decreasing skin friction drag inside the engine. It is desirable to do this while

minimizing the total pressure loss due to fuel mixing. Ignition and flameholding in high speed flows are also major design challenges.

A variety of fuels could be used for a scramjet vehicle. Hydrogen is attractive due to its high energy to weight ratio, which maximizes the allowable payload and vehicle weight for a given mission. The use of more conventional hydrocarbon fuels like JP-7 allows simpler packaging due to their high volumetric energy density and liquid state at atmospheric conditions. The use of other hydrocarbon fuels is also possible

Due to the high cost of experimental testing at such extreme conditions, advanced computational methods are needed to design an efficient scramjet combustor. In order to design injectors with enhanced penetration and mixing, current levels of understanding must first be significantly improved. One area that has been identified as needing further study is the influence of injectant molecular weight and so that is a primary focus of this study.

II. TECHNICAL BACKGROUND

A multitude of experiments have been performed in the field of injection in supersonic flow using numerous techniques. A representative sample of previous works is listed here as Refs. [3]–[18]. Extensive reviews of injector mixing characteristics are given in Refs. [19] and [20].

The injection of fuel into a scramjet is essentially the injection of a jet into a high speed flow. In front of the injection a three dimensional bow shock forms where the high speed flow is blocked by the lower speed injectant. This forms a subsonic mixing region just in front of the injection point. A horseshoe vortex wraps around the jet and wake vortices stretch along the jet to form a counter rotating vortex pair (CVP) downstream. A series of spanwise rollers is periodically generated and convected downstream with the flow. Yuan et al[21] showed that the generation of these vortices is caused primarily by Kelvin-Helmholtz instability. Unfortunately this is suppressed by compressibility effects, reducing turbulent mixing. Figure 2 below shows a diagram of the major structures.

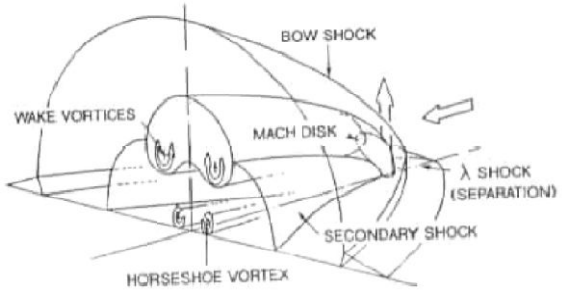

Figure 2. Diagram of transverse jet-crossflow interaction structures (image from ref 22)

The boundary layer can obviously play an important role in this process. Near the wall viscous effects dominate the flow. Cortelezzi and Karagozian showed in a computational study that with a thicker the boundary layer the penetration was higher the mixing was reduced in the near field[23]. This is because the lower velocity fluid in the boundary layer decreases the momentum transfer between the free stream and the jet.

In most experimental studies the injectant is highly pressurized to ensure choked flow through the injector itself and make the injection properties independent of free stream conditions. This results in the jet being under-expanded when it enters the flow. A barrel shock is formed around its interface with a Mach disk being formed slightly downstream which decreases the speed and increases the pressure of the jet[24].

The one parameter that has been shown to have the most effect on the penetration of the plume is the jet to free stream momentum ratio, $\bar{q}$. The use of this term to parameterize the flow was first suggested by Schetz and Billig[25] in 1966 who used this parameter to develop an approximate model for penetration based on this parameter for injection normal to the flow. This early model was evaluated favorably by Orth and Funk[26] against empirical data. Later studies by Papamoschou and Hubbard[27] demonstrated in 1992 that penetration was strongly dependent on $\bar{q}$ and essentially independent of other quantaties which might be expected to be important, such as Mach number and pressure ratio. This same conclusion was supported by Gruber et al.[28] who also found that data for various injection conditions would collapse into a single curve when normalized for $\bar{q}$. Gruber et al. also proposed a power low approximation of penetration based on $\bar{q}$. The higher the momentum of the injection jet, the higher the penetration generally. For some injector geometries, such as diamond shaped injectors, there are other effects that take place at high momentum ratios that become more important. Hirano et al found that above a certain ratio 'axis switching' can occur in which the reflection of expansion waves at the jet boundary forms cell structures that increase lateral spreading[29].

Many attempts to improve this mixing process through geometry of the injector and the flow qualities of the jet, but there is a relative dearth of studies of the impact of what effect the injectant properties have on the mixing process. Ben-Yakar et al[24] conducted a study where both hydrogen and ethylene were injected into a Mach 3.4 flow with $\bar{q} = 1.4$ and found that the higher molecular weight ethylene penetrated further and mixed more thoroughly than the hydrogen did. They attributed this to differences in the large scale vortical features in each case. Molecular weight could affect the formation of these periodic wake vortices because Kelvin-Helmoltz is affected by compressibility, and molecular weight affects the Mach number by altering the speed of sound. Gruber et al.[28] identified the same increase in periodic vortex generation and mixing when comparing air and helium injection, although they did not identify any significant change in penetration.

If a shock is impinging on the injection jet, as is quite likely given the large number of reflected shocks in a scramjet combustor, then this creates a misalignment between the density gradient and the pressure gradient and generates vorticity through baroclinic torque. This situation is called Richtmyer-Meshkov instability and the effect is described analytically by Bjerknes theorem:

$$\frac{d\Gamma}{\mathrm{dt}} = \int \frac{1}{\rho^2}(\nabla\rho \times \nabla P)dA$$

Because this effect is caused by the radial density gradient between the jet and the working fluid, it is greater if the injectant gas is lighter or heavier than the working fluid.

A better understanding of these effects is necessary to improve the utility of current CFD codes in the design of effective scramjet combustors. Specifically, additions need to be made to Reynold's Averaged Numercal Solver (RANS) code turbulence models to predict the effect of variations of the Schmidt and Lewis numbers, the ratios of mass diffusivity and thermal diffusivity (respectively) to mass diffusivity. Since molecular weight has an effect on mass diffusivity, this must be taken into account in order to improve the accuracy of current models[30]. This need is a primary motivation for this study.

III. EXPERIMENTAL METHODS

A. FACILITIES

Experiments were performed in the Virginia Tech supersonic wind tunnel with a Mach 4 nozzle. This nozzle was chosen in order to represent the combustor Mach number of a scramjet traveling with a flight Mach number of approximately 12. This is a blow-down type tunnel with a 23 x 23 cm test section and a maximum run time of approximately 25 seconds. The tunnel is charged by an Ingersoll-Rand, type 4-HHE-4, water cooled, four stage compressor equipped with a dryer and separator to remove water vapor and oil during operation. Compressed air is stored in two tanks with a combined volume of 23 cubic meters. During runs, these tanks feed into a plenum through a pneumatic butterfly valve which is controlled by a PID program in order to maintain a constant pressure. The pressure typically varied by less than ± 35 kPa from its set point of 1034 kPa during the initial oscillations, settling within 1% of the desired value. The total temperature was approximately 300 K.

The injector and sampling station were installed in the floor of the test section as shown in Figure 2. A circular, single-port, flush wall injector was used for these experiments. The injector had a diameter $d_j = 3.23mm$, and was inclined at an angle of 30 degrees to the wall. This was chosen to be representative of a basic injector that might be considered for a true scramjet combustor. Dimensions were normalized to the effective diameter:

$$d_{eff} = \sqrt{C_d} d_j$$

Where the discharge coefficient $C_d = 0.88$, giving $d_{eff} = 3.03mm$ A diagram of the injector insert is shown in Figure 3.

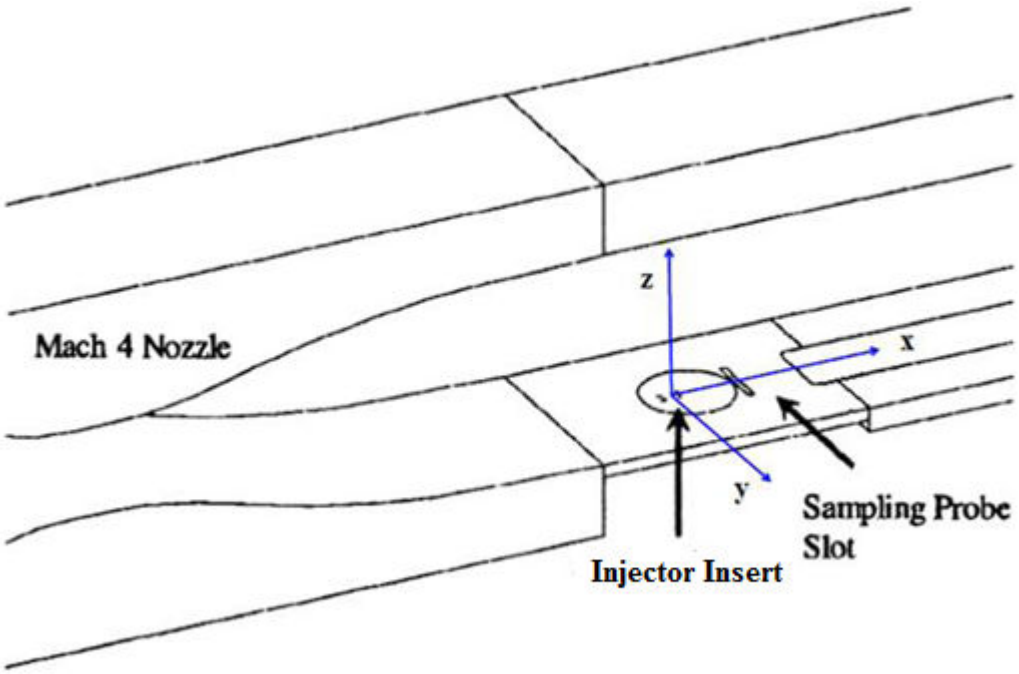

Figure 3. Experimental set up

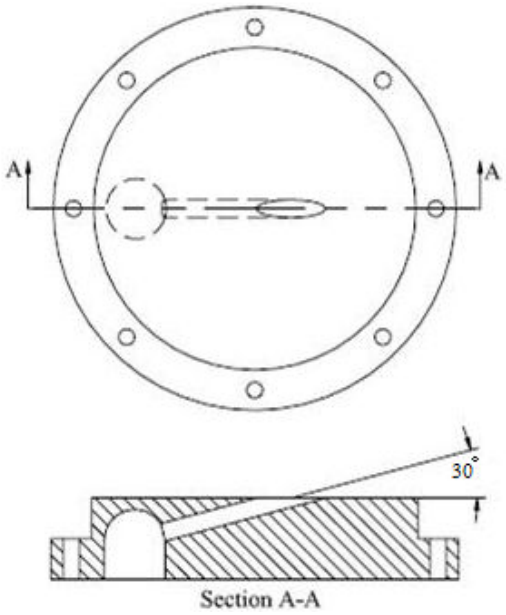

Figure 4. Single circular hole injector insert, diameter 3.23 mm, flow left to right

Probes were used to measure the flow field downstream of the injector. The measurement probes were mounted on a traverse system underneath the test section, penetrating into the test section through slots as shown in figures 3 and 5. The slots allowed the probes to be traversed in both dimensions perpendicular to the flow.

The boundary layer thickness at the measurement station has been investigated in order to characterize the free stream conditions, and it has been found to be approximately 20mm. This survey was performed using the 5-hole probe and traverse system described later.

For the shock interaction studies, a two-dimensional shock generator was used to create an oblique shock of 19±0.5 degrees, generating a pressure ratio of 1.65±.05, to impinge upon the injection jet and associated vortex structures. The shock generator consist of a wedge with an included angle of 12 degrees and a 20cm wide leading edge attached to a sting mount as shown in Figure 4. This shock strength is intended to be representative of a reflected shock that could be present in a scramjet combustor.

Figure 5 also shows the concentration probe mounted downstream of the injector. The five-hole probe was mounted through the same slot as the forward strut of the concentration probe.

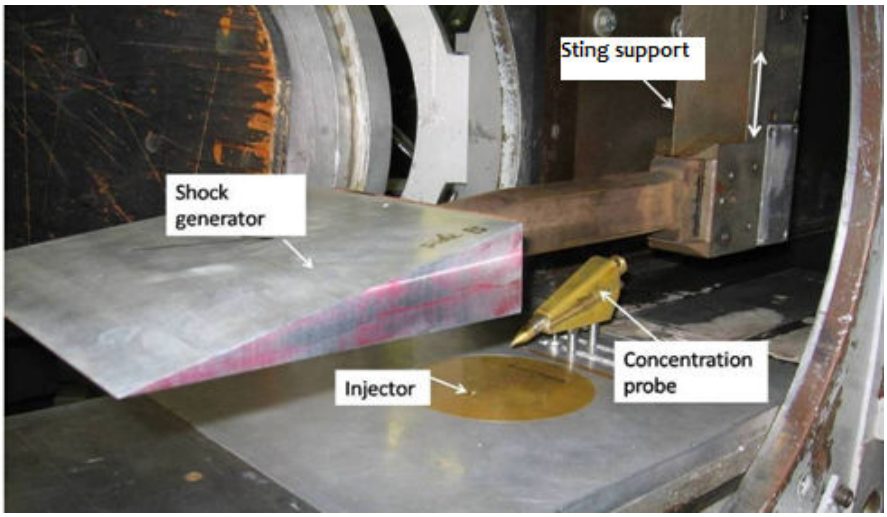

Figure 5. Shock generator in test configuration

B. INJECTION CHARACTERISTICS

Injection was sonic for all injectants, as would be the case in a scramjet combustor. Choking the injector has the effect of preventing the tunnel conditions from influencing the injection parameters. In order to compare the results for injection of differing gases, the jet to free stream dynamic pressure ratio, defined on the following page, was held constant at 2.1 for all injectants.

$$\bar{q} = \frac{(\rho u^2)_j}{(\rho u^2)_\infty} = \frac{(p\gamma M^2)_j}{(p\gamma M^2)_\infty}$$

This was done because $\bar{q}$ has generally been found by several experimenters[27-28] to be sufficient in predicting penetration in the presence of pressure and velocity changes, so keeping $\bar{q}$ constant should make molecular weight the only untested variable between the injectants. In order to hold the dynamic pressure ratio constant, the injection mass flow $\dot{m}_j$, was varied.

$$\dot{m}_j = \rho_j u_j A_j$$

The injection characteristics resulting in $\bar{q} = 2.1$ are shown in table 1:

Table 1. Injection properties

Injectant	$\bar{q}$	$\dot{m}_j$	P_t	T_t
Methane	2.1	6.7 g/s	484 kPa	300 K
Air	2.1	10.0 g/s	523 kPa	300 K
Carbon Dioxide	2.1	11.8 g/s	555 kPa	350 K

Carbon dioxide injection presented a potential problem because at low temperatures it can undergo deposition and become solid. To prevent this a 2 kW heater was used to raise the temperature to 350 ± 10 K. Mass flow rate was calculated by measuring the pressure drop across an orifice flow plate, and was maintained to within $\pm 5\%$ of the nominal value during all runs.

C. PROBE TRAVERSE AND DATA ACQUISITION

Data was taken by means of probes mounted on a two axis Velmex Unislide traverse system. The traverse speed was 5mm/sec, which allowed an entire vertical section of data to be taken in each run with 200 millisecond stops at each vertical station, so that at least 50 samples could be averaged to produce the data at each point. Between runs, the traverse was moved laterally to the next horizontal station. Data was recorded on a PC with a 16-channel, 16-bit A/D converter (AT-MIO-16XE-50), and a 64-channel multiplexer (AMUX-64T) both built by National Instruments with a built-in cold-junction compensator for temperature measurements. Data was taken at 500 Hz. The probe position was controlled by a LabView program integrated into the tunnel control program.

D. CONCENTRATION PROBE

The first probe used was a gas species concentration probe developed by Dr.Ng[31] and his associates at Virginia Tech. A diagram of the probe is shown in Figure 6. The probe used three measurements taken within its housing to determine the molar fraction of a binary mixture of gases. Temperature was measured with a K-type thermocouple, and pressure was measured with an externally mounted pressure transducer connected to an internal port. Additionally voltage was recorded from a TSI 1210-50 platinum hot-film sensor using a Dantec Type 56C17 constant temperature anemometer and a DISA Type 56C01 CTA bridge. The diameter of both the sampling plane and the choked orifice was 0.63 mm. The flow channel expands to a diameter of 3.8mm so that a normal shock is formed in front of the sensors. Mechanical aspiration by means of a vacuum pump ensures that the orifice remains choked, so that a stream tube equal in area to the probe tip enters undisturbed. The diverging internal flow section creates a very low velocity in the region of the sensors, so that conditions can be treated as stagnation conditions.

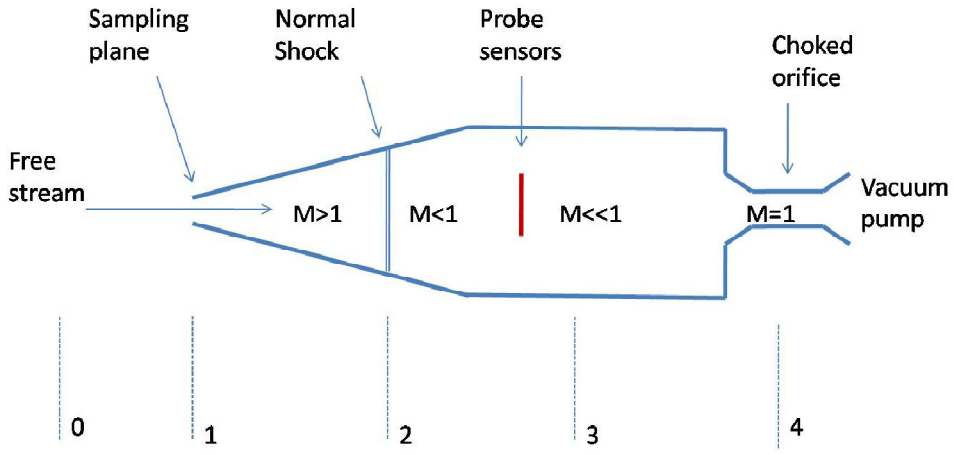

Figure 6. Diagram of the concentration probe

The mass flow through the choked orifice can be expressed as

$$(\rho u)^* = \frac{P_t C^*}{\sqrt{T_t}}$$

Where C^* is a function of sonic conditions defined as

$$C^* = \sqrt{\frac{\gamma W}{\mathbb{R}}}\left[\frac{2}{\gamma+1}\right]^{\frac{\gamma+1}{2(\gamma-1)}}$$

Where W is the molecular mass, $\mathbb{R}$ is the universal gas constant and γ is the ratio of specific heats. Along with the known probe geometry, continuity allows the mass flux at the measurement plane to be related to the sonic conditions by the ratio of the areas of the choked orifice A^* and the area of the measurement plane by

$$\rho u = \frac{P_t C^*}{\sqrt{T_t}} \frac{A^*}{A_c}$$

With the temperature and pressure known from measurements and the geometry being fixed the mass flow is a function of the composition of the mixture through W and γ.

The rate of heat transfer q_f for the hot film at the measurement plane is related to the film current I_f and the film resistance R_f as shown below

$$q_f = I_f^2 R_f$$

The voltage response is related to the film current for a constant temperature anemometer is:

$$I_f = \frac{V}{R_f + R_s}$$

Where R_s is the series bridge resistance. To relate the heat transfer rate of the hot film sensor to the temperature of the surrounding fluid the Nusselt number, defined below, is utilized. l is the sensing length of the hot film and k is the thermal conductivity of the gas mixture.

$$Nu = \frac{q_f}{\pi k l \left(T_f - T_t\right)}$$

This can also be written as:

$$Nu = \left(\frac{R_f}{R_f - R_s^2}\right) \frac{V^2}{\pi k l (T_f - T_{t)}}$$

The Nusselt number can also be expressed in terms of Reynold's number and two empirical constants that depend only on the gas composition.

$$Nu = a(Re)^b$$

Combining these two forms the hot film voltage can be expressed as:

$$V^2 = \frac{\left(R_s + R_f\right)^2}{R_f} \pi l k a \left(\frac{d P_t A^* C^*}{\mu \sqrt{T_t} A}\right)^b \left(T_f - T_t\right)$$

All parameters on the right side of this equation with the exception of T_t and P_t are a function either of the geometry or the properties of the gas mixture, and hence the relative concentrations of its constituent species. Since the total pressure and temperature are measured by the probe along with the hot film voltage, the relative concentrations of the gas mixture is uniquely determined.

In order to determine the coefficients a and b the probe was calibrated by connecting it to a tank with the desired gas mixture in known concentrations at varying pressure. The tank was first pumped to a vacuum, then filled with controlled partial pressures of the desired species. The tank was initially pressurized to 276 kPa with this known mixture, and then emptied slowly with the aid of the vacuum pump so that the calibration would cover the necessary range of pressures. The probe is sensitive to variations in the gas constant, i.e. mixture molecular weight, so it is less sensitive for methane in air mixtures than for helium in air mixtures as shown in figure 7.

This calibration could only be performed successfully for methane. The molecular mass ratio was only 1.5 between CO_2 and air compared to about 2.0 for methane and air. Also the ratio of viscosities was only 1.2 between CO_2 and air compared to more than 1.6 methane and air. Since the probe is sensitive to variations in these properties as these ratios approach 1 the probe loses effectiveness. The effect of this was that the different calibration curves became indistinguishable from one another as shown in figure 7. This limited the availability of mass fraction contours to methane injection only.

A)

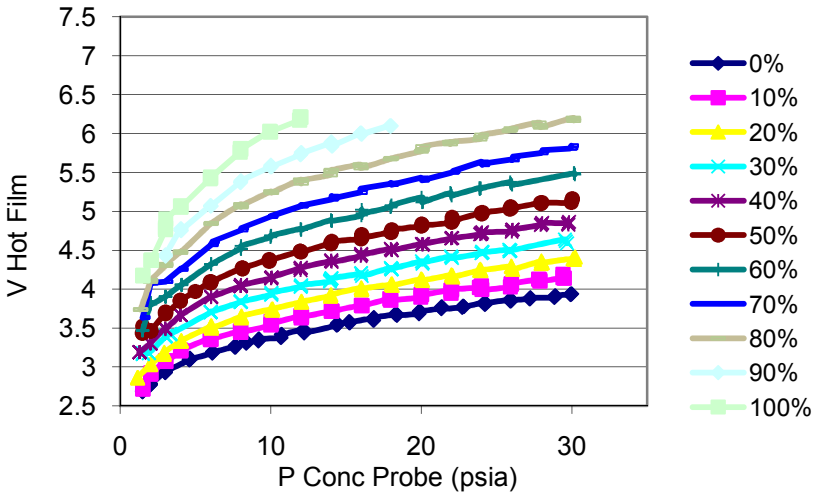

Figure 7. Concentration probe calibration for A) helium in air, B) methane in air, and C) carbon dioxide in air

B)

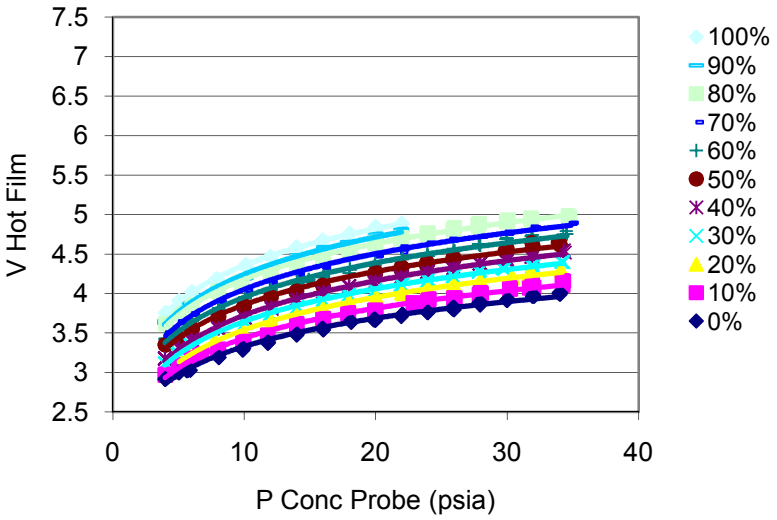

C)

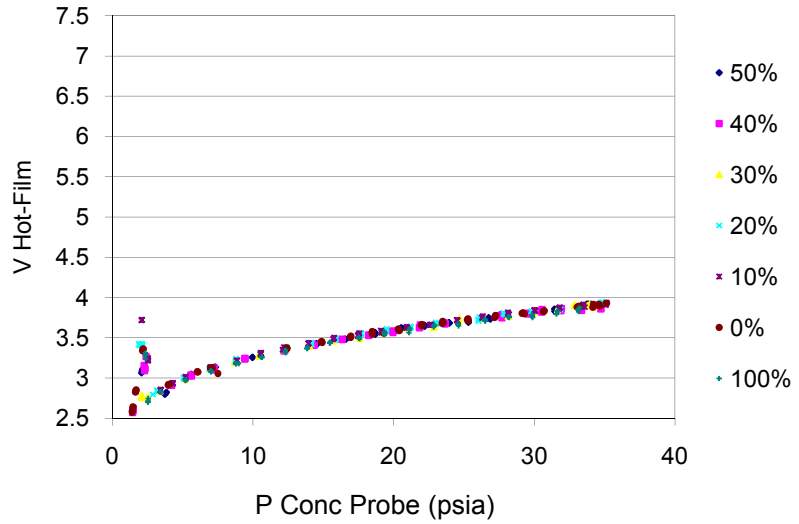

Figure 7. Continued

The uncertainty of the probe was determined by comparison of the computed mass fraction during calibration to the known fraction during each run. The largest standard deviation between the probe measurements and the nominal value of any of the runs was 0.016, which means that more than 95% of the measured values would be within 0.032 of the nominal values. This is the dominant source of error as all nominal calibration values were set within 0.001 of the desired concentration, so essentially all measured values were within 0.03 of the actual concentration.

E. FIVE-HOLE PROBE

The other probe used in this study was a five-hole probe designed at Virginia Tech by Luca Maddalena[17] based on the initial work of Centolanzi[32]. The conical tip is 1.65mm in diameter with a pressure port at the tip and four more arrayed around the cone surface. The pressure ports have an inner diameter of 0.419 mm and each contains an Endevco model 8507-C-50 miniature piezoresistive transducer as shown in Figure 8. The semivertex angle is 45 degrees. Having imbedded transducers allows for a 99% step response time of only 11 milliseconds. Its power supply output is ±13.5 VDC which is filtered through a two-stage active filter and regulated to 10 V for sensors and ±12 V for amplifier modules. Individual amplifier gain is set for the full range of sensors to ± 5 V.

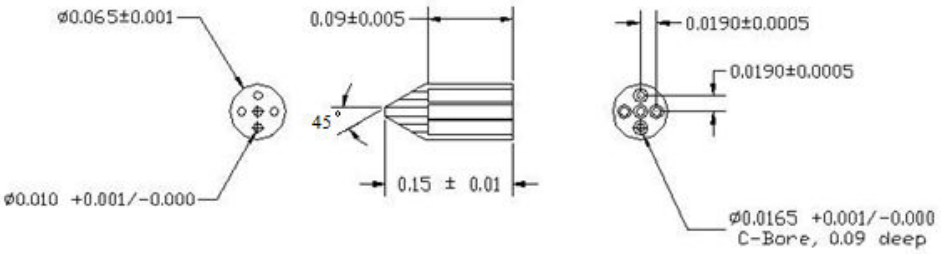

Figure 8. Five-hole probe tip (dimensions in inches)

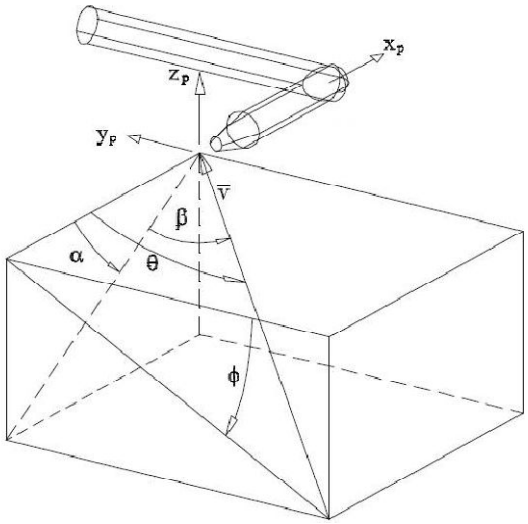

Figure 9. Five-hole probe tip showing angle definitions used in data reduction

Through a calibration process, the relative pressures can be related to the local flow angles and Mach number. To determine the angularity two coefficients are defined:

$$C_{p\eta} = \frac{P5 - P3}{q}$$

$$C_{pz} = \frac{P4 - P2}{q}$$

Where $P1, P2, P3, P4, P5$ are the port pressures and q is the dynamic pressure. These coefficients can be uniquely related to pitch, θ, and roll, φ. Angle definitions are shown in figure 9.

The five-hole probe was calibrated in the Mach 3.1 Supersonic Free Jet Facility at Virginia Tech which was designed by Maddalena for that purpose. The probe was mounted on a support that could pivot the probe in both pitch and yaw. During a period of continuous run, the probe was moved through a range of angles of ±18 degrees in both axes with measurements taken at increments of 0.9 degrees up to 9 degrees and 1.8 degrees for the remainder of the range. A quarter of the full calibration map consisting of 961 points is shown in Figure 10. Each line represents a constant angle, each concentric line representing a pitch angle and each radial line a yaw angle.

An analysis of a probe of this type showed agreement to within 0.333% for calibration performed at a Mach number of 3.55 and a Mach number of 21, so the angularity map can be taken to be independent of Mach number[33]. In order to calibrate for Mach number, the probe was traversed through the boundary layer of the VT supersonic wind tunnel where the Mach number was measured separately using a 10 degree cone-static probe and a Pitot probe mounted together. The ratio of the center port pressure to the average of outer port pressures $P1/_{PA}$ was then plotted vs. Mach number and a power curve fit was employed as shown in Figure 11. Once the Mach number and the flow angularity have been determined, then the flow components can be computed as:

$$M_x = -Msin(\theta)\sin(\phi)$$

$$M_y = -Msin(\theta)\cos(\phi)$$

$$M_z = Mcos(\theta)$$

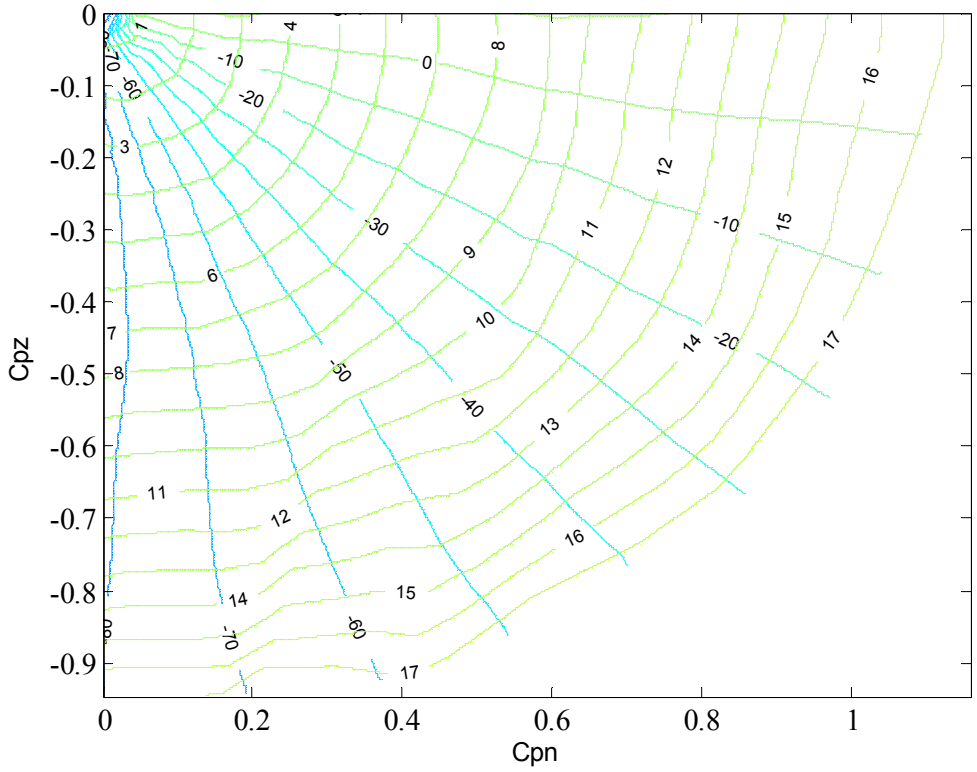

Figure 10. Five-hole probe calibration map

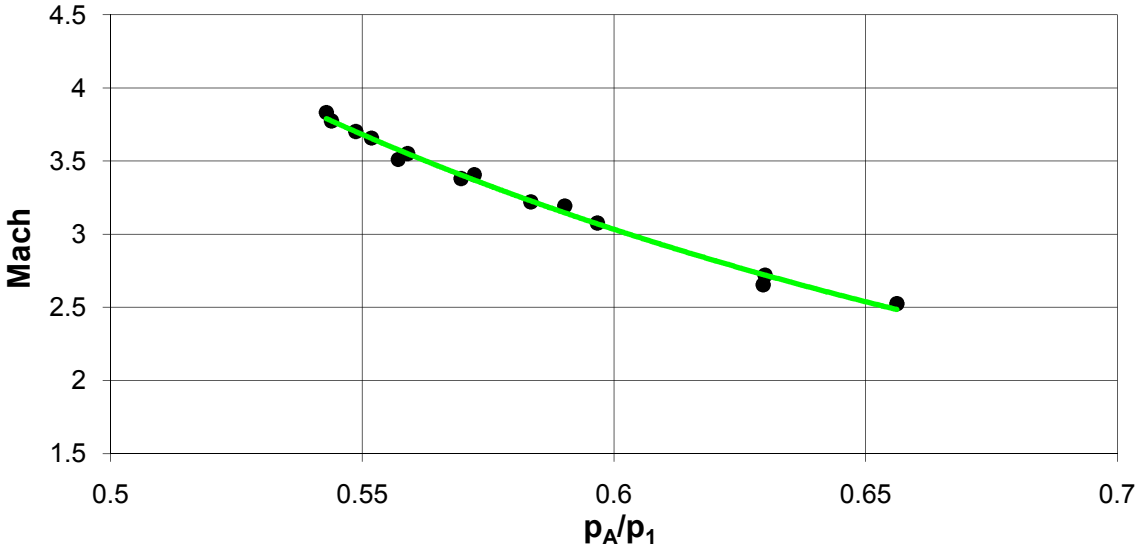

Figure 11. Five-hole probe Mach number calibration

Since $^{P1}/_{PA}$ is a function of flow direction, an additional iteration is performed using a correction factor map to increase the accuracy of the computed Mach number.

Because this calibration curve is for air, error is introduced when sampling a mixed flow of air and methane in the jet plume, where the ratio of specific heats, γ, is not identical to that of air. In order to characterize this error, Taylor-McColl solutions were performed for the similar situation of a 45 degree half-angle cone. As shown below in Figure 12, this analysis predicts the error generated by representative mixtures for the average plume concentration and the maximum concentration at any of the points sampled. At these conditions $\gamma = 1.37$, and $\gamma = 1.33$, respectively.

The error in percent of nominal Mach number declines with decreasing Mach number. Since the high concentrations of methane occur inside the injection plume where Mach number is low, the error is minimized. The maximum concentrations occur where the Mach number is approximately 2.5, leading to a maximum error of 5% in Mach number.

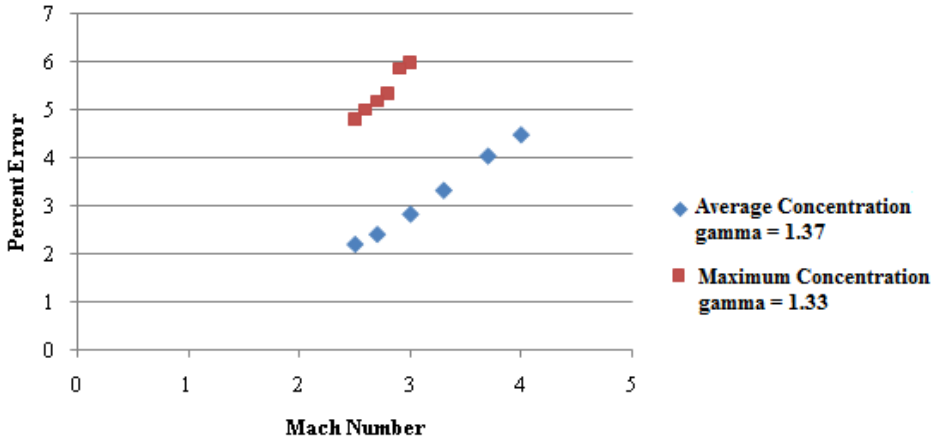

Figure 12. Error introduced in Mach number results by gas mixtures inside plume

F. SHADOWGRAPH & SCHLIEREN PHOTOGRAPHY

In addition to probe surveys, shadowgraph and schlieren photographs were used to visualize flow structures and shock impingement. Shadowgraph photography takes advantage of the refraction of light caused by density gradients. When a beam of collimated light is projected through the test section, the light will refract towards the direction of increasing density, making these areas

appear darker when the light is focused into an image. A General Radio Model 1538-A strobotac was used as a light source, and the beam was collimated with a 30.5 cm diameter parabolic mirror with a focal length of 203 cm. Another identical mirror focused the light beam onto a digital camera. The addition of a knife edge placed at the focal point of the mirror behind the subject of the photograph creates a schlieren photograph, and increases the sensitivity of the technique. For schlieren photographs an ABET Technologies LS-150-Xe xenon light was used, with the same mirrors.

IV. EXPERIMENTAL RESULTS

Concentration measurements were taken 13.9 d_{eff} downstream of the injector, and all other measurements were taken 17.2 d_{eff} downstream. The different locations were necessitated by the dimensions of the various probes and the geometry of the wind tunnel. Height above the wall and horizontal distance were selected to be sufficient to capture the flow field of the plume, approximately $Y_{max} = \pm 4\ d_{eff}$ from the injector centerline and $Z_{max} = 8\ d_{eff}$ above the wall. Data was taken as close to the wall as probe geometry allowed. Data shown below this level is an extrapolation based on wall assumptions, and is delimited by a red line on the plots. The uncertainty in the grid origin location is $\pm 0.2\ d_{eff}$, and the uncertainty of grid points relative to each other is $\pm 0.0001\ d_{eff}$.

Data is presented for three cases: 1) injection into an undisturbed free stream, 2) injection with the shock impinging 4.5 ± 0.2 diameters upstream of the injector center, and 3) injection with the shock impinging 2.5 ± 0.2 diameters downstream of the injector center. Figure 13 shows a comparison of these three cases in the form of shadowgraph photography, which allows the bow shock in front of the injector and the wedge-generated shock to be clearly seen. It is also apparent that there is no unintended interference to the flow in the jet plume from the shock generator or its wake. Carbon dioxide data was taken only for case 1).

A)

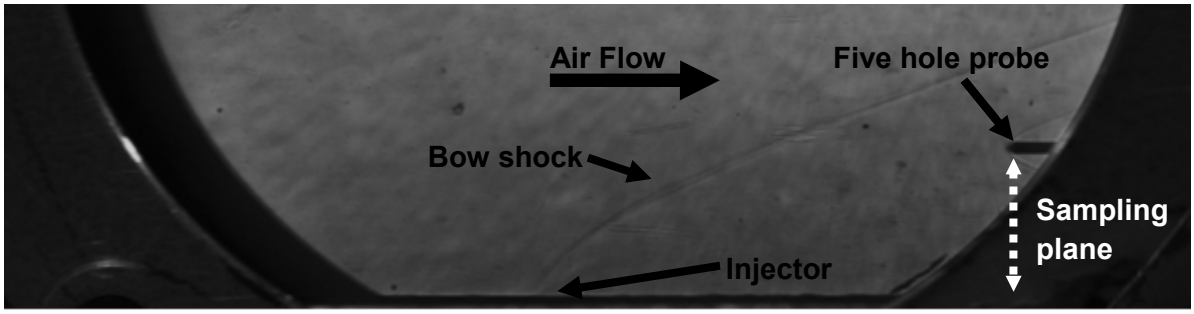

B)

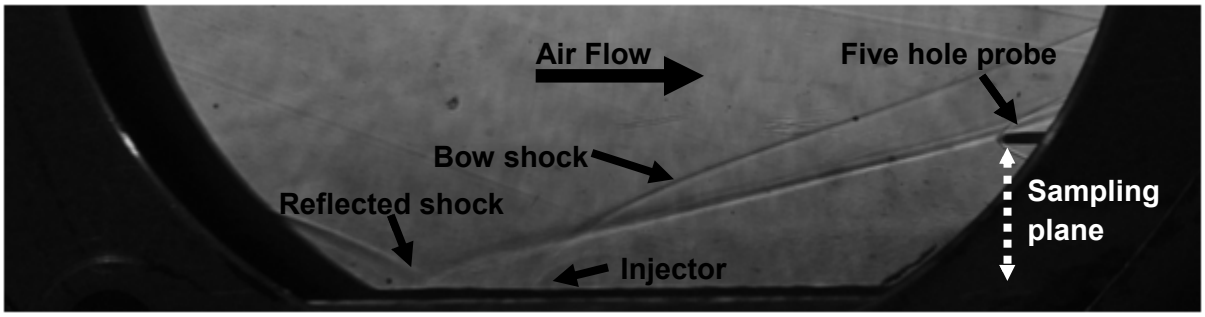

C)

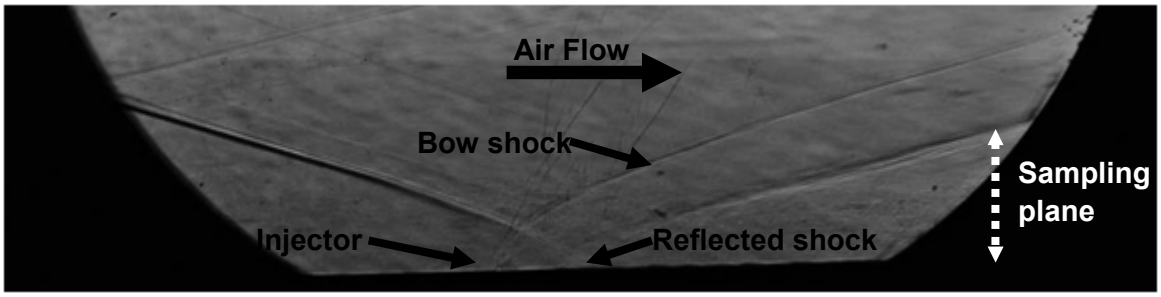

Figure 13. Shadowgraph photographs of air injection into A) undisturbed free stream, B) shock reflection upstream of injector, C) shock reflection downstream of injector

A. SCHLIEREN PHOTOGRAPHS

For the undisturbed case schlieren photographs were taken of each injectant. These photographs are shown in figure 14. It can be seen that the bow shock created by the injection of CO_2 is significantly higher and stronger than that generated by the injection of air. The plume also seems to penetrate significantly higher.

A)

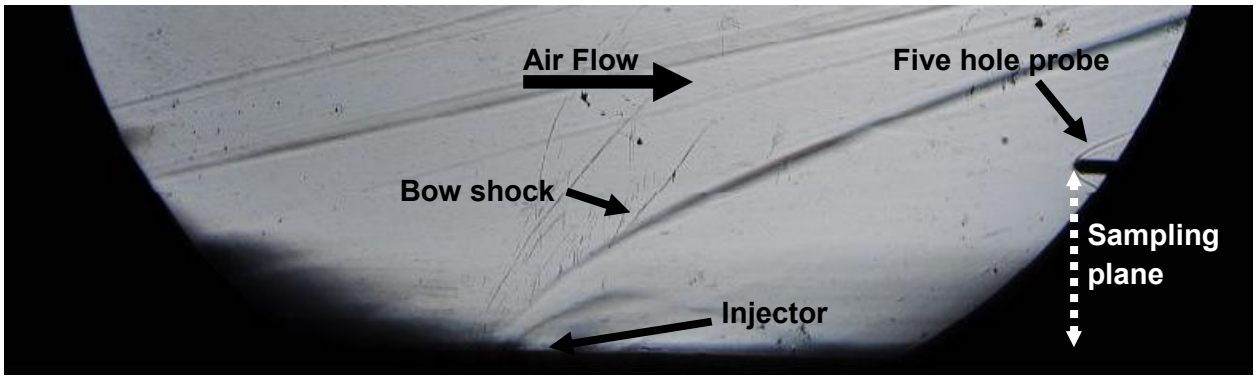

B)

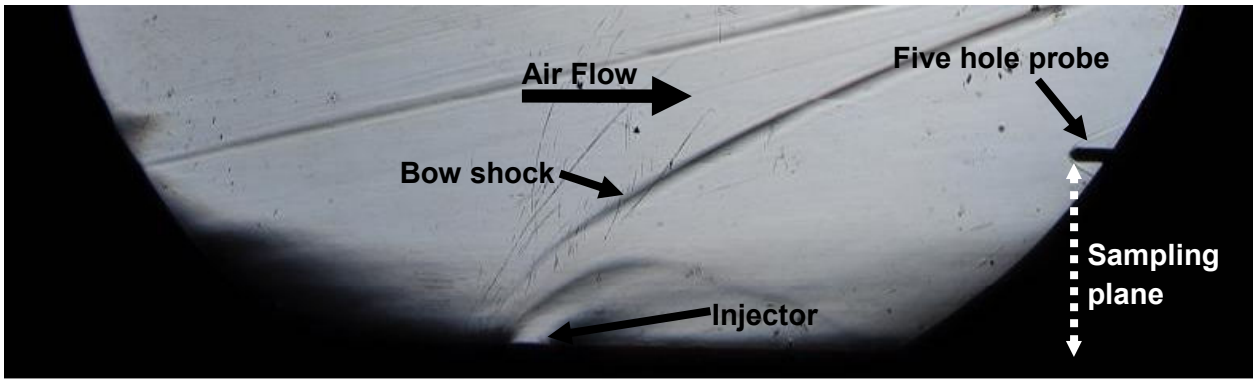

Figure 14. Schlieren photographs of injection A) air and B) carbon dioxide

B. MACH NUMBER CONTOURS

The Mach Number data computed from the five-hole probe surveys for both air injection into air and methane injection into air is presented as a series of contour plots in Figures 15-17. Mach number surveys of carbon dioxide into air were only performed for the no-shock case; these results are included in figure 15. The uncertainty in the computed Mach number is $\pm 5\%$. The

region influenced by the injection plume can be seen as an area of reduced Mach number as the relatively low velocity injectant mixes with the high speed flow. This series of measurements complements those of Maddalena[17], who performed experiments in the same facility with helium injection, in both undisturbed flow and with shocks reflecting at 2, 8 and 16 d_{eff} downstream of the injector. To provide a quantitative measure of the penetration height the Mach number defect is defined as:

$$M_* \equiv M_\infty - M$$

Where M_∞ is the nominal free stream Mach number uninfluenced by the presence of injection. In the case of the undisturbed free stream this is simply the nominal free stream Mach number or 4. In the cases with shock impingement it is the Mach number away from the wall but still behind the shock, 3.7. The vertical location of the centroid of this quantity is then used as a measure of penetration height as follows:

$$\bar{z}_{M_*} = \frac{\int y M_* dA}{A} \approx \frac{\sum y M_* \Delta x \Delta y}{A}$$

The approximate summation was performed using each data point as an element to yield the comparison shown in table 2. These results seem to show that the higher molecular weight air penetrated further in each case for the same momentum flux ratio.

Table 2. Global parameters deduced from Mach number contours

No Shock	Injectant	CO2	Air	CH4
	$\bar{y}_{M_*}$	3.52	2.64	2.51
Shock Upstream x/d_{eff} = - 4.5	Injectant		Air	CH4
	$\bar{y}_{M_*}$		2.51	2.17
Shock Downstream at x/d_{eff} = 2.5	Injectant		Air	CH4
	$\bar{y}_{M_*}$		1.75	1.68

A)

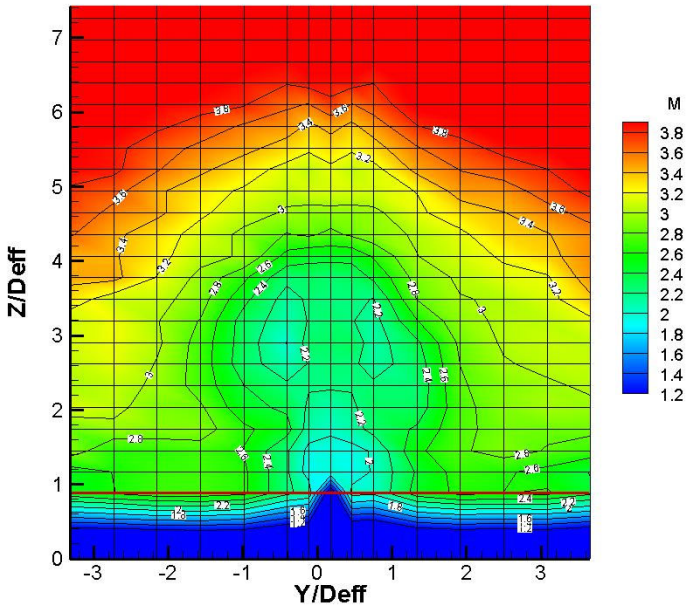

B)

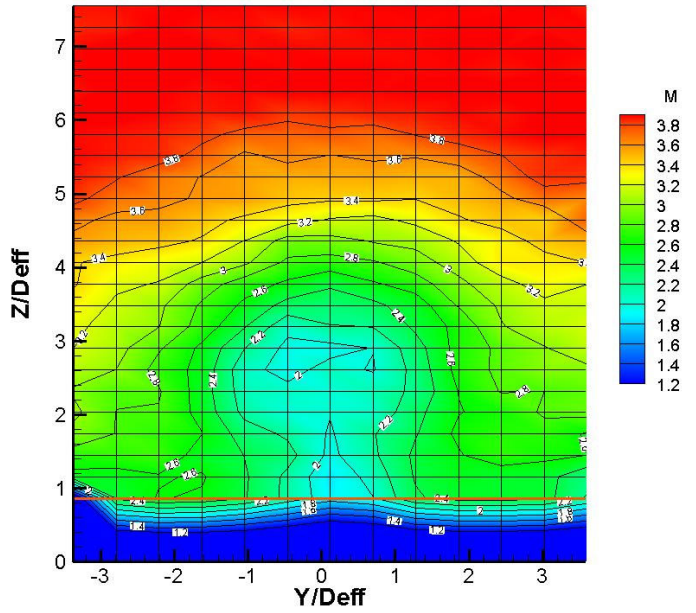

Figure 15. Mach number contours for injection into undisturbed flow, A) air into air B) methane into air and C) carbon dioxide into air (Data below the red line is extrapolated)

C)

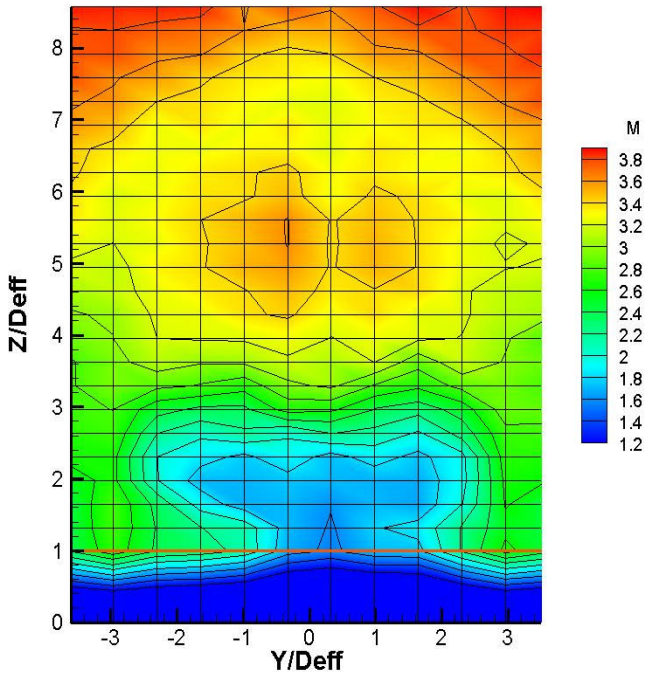

Figure 15. continued

The contour pattern created by CO_2 injection differs notably from that of both methane and air injection. The survey reveals a lower region of very low Mach number but a higher region of slightly reduced Mach number. This latter region seems to be associated with the bow shock of the jet. The schlieren photographs comparing air and methane injection show a considerably steeper bow shock created by CO_2 injection, which creates a larger space between the jet itself and the bow shock. This could indicate that the heavier gas is mixing more slowly, thus creating a locally slower and denser region that creates a larger bow shock. A lower and wider plume would also create a more two dimensional bow shock, which would appear steeper in the streamwise vertical plane.

A)

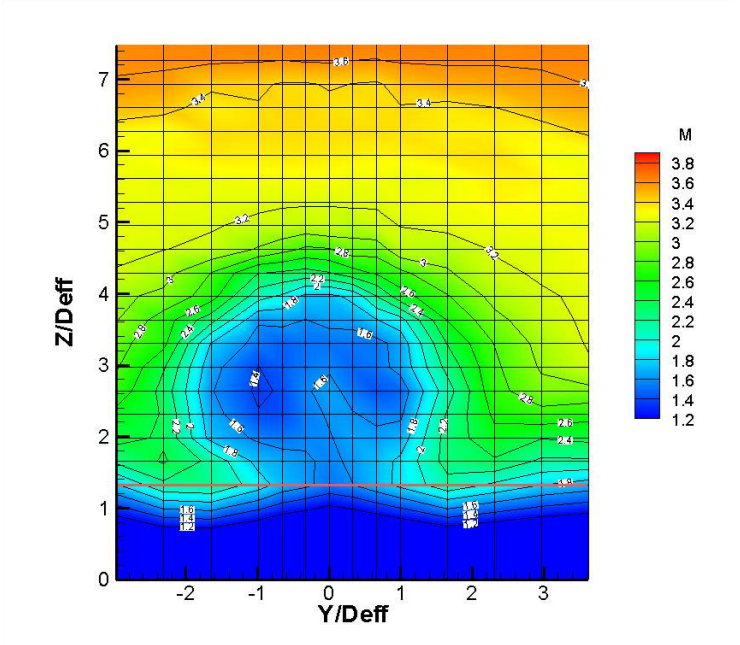

B)

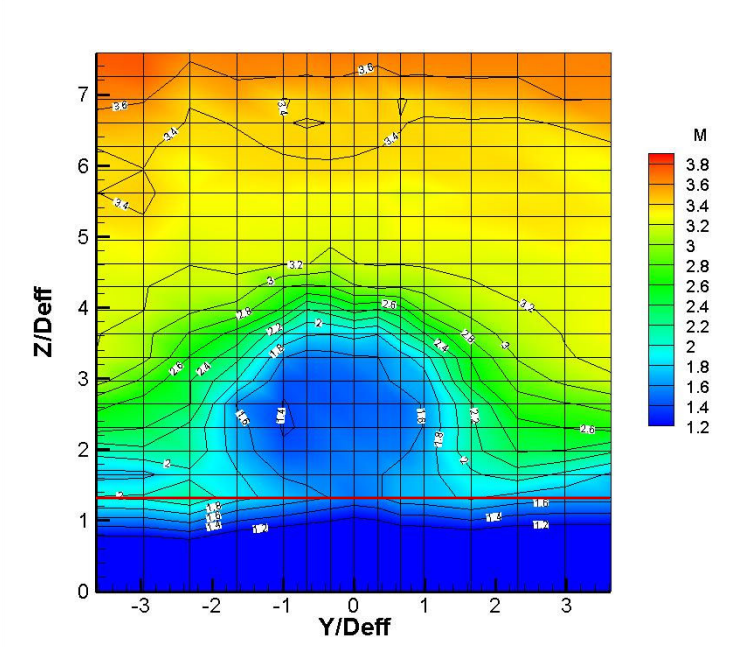

Figure 16. Mach number contours for injection with shock impinging upstream of injector, A) air into air B) methane into air (Data below the red line is extrapolated)

A)

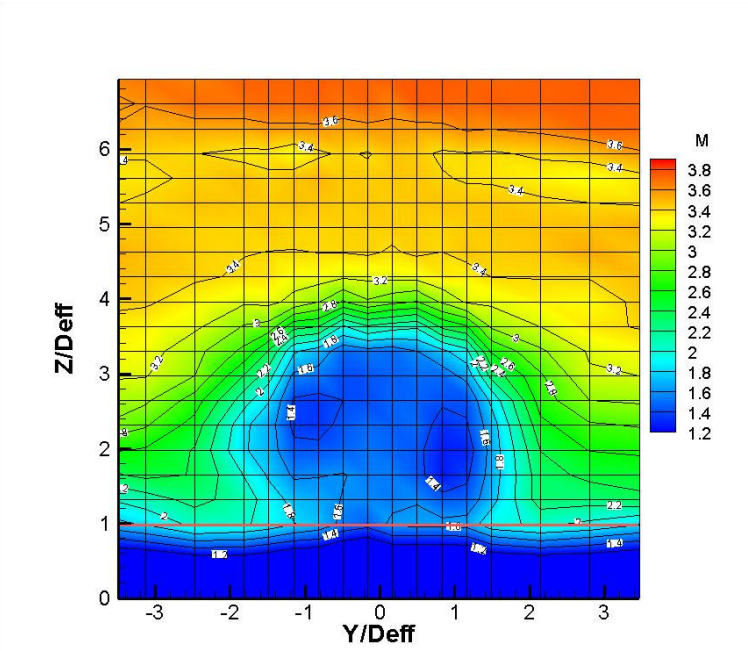

B)

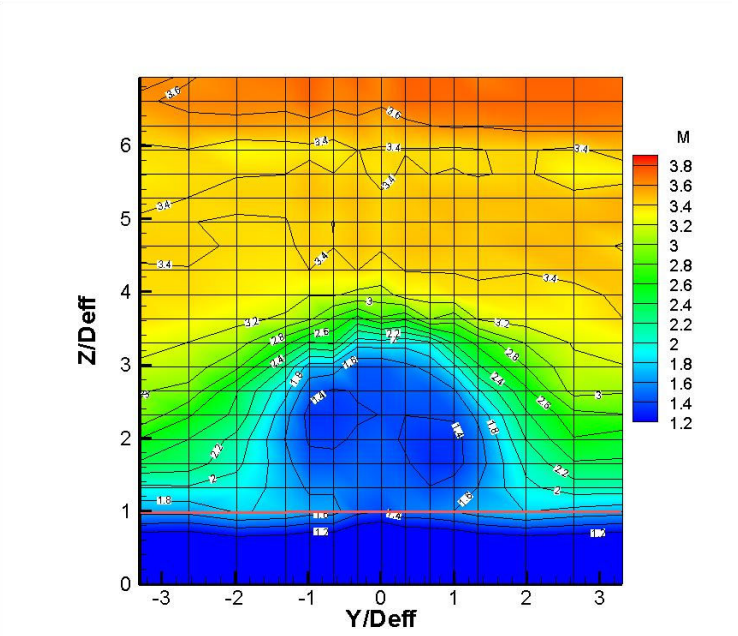

Figure 17. Mach number contours for injection with shock impinging downstream of injector, A) air into air B) methane into air (Data below the red line is extrapolated)

C. MACH NUMBER COMPONENTS

The Mach number in the cross stream directions was computed for each case from the five-hole probe surveys as described earlier. The results are displayed as a grid of vectors each representing a single point showing the direction and relative magnitude of the cross stream Mach number throughout the flow (Fig 18-20). The uncertainty in the flow angle is $\pm 0.5^{o}$. The most notable feature of the flows is the counter-rotating vortex pair (CVP) which dominate the flows in the region of the plume. These vortices are formed on the lateral edges of the injection jet by the skewed mixing layers there, see Yuan[21]. Also, in the downstream shock impingement cases in Fig. 18 at the height where the measurement plane crosses above the reflected shock, one can see the change in the vector pattern as the free stream flow angle turns 5.3 degrees to become parallel with the wall.

A)

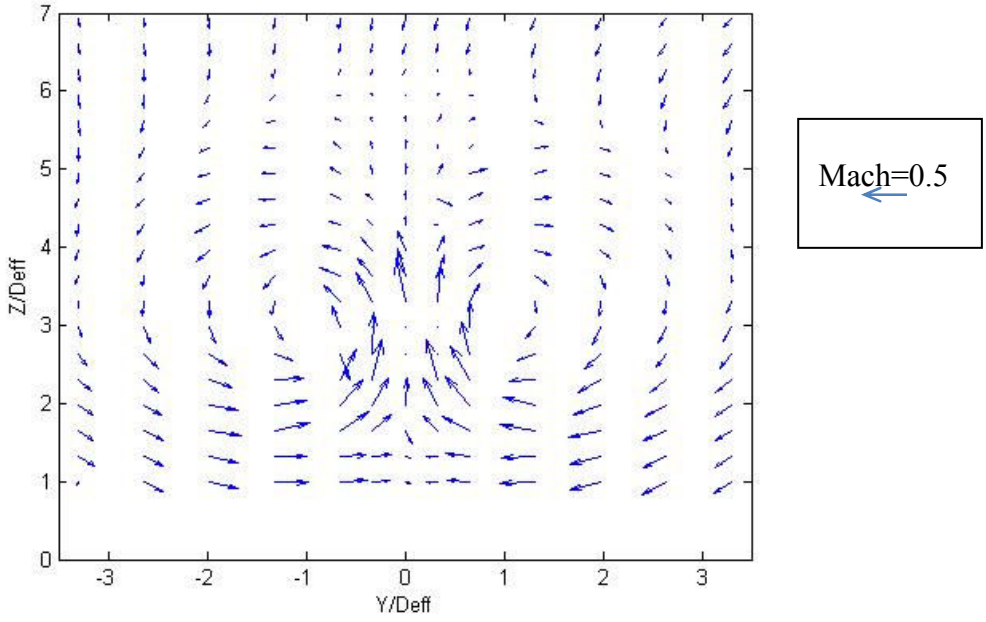

Figure 18. Transverse Mach number components for injection into undisturbed flow, A) air into air B) methane into air C) carbon dioxide into air

B)

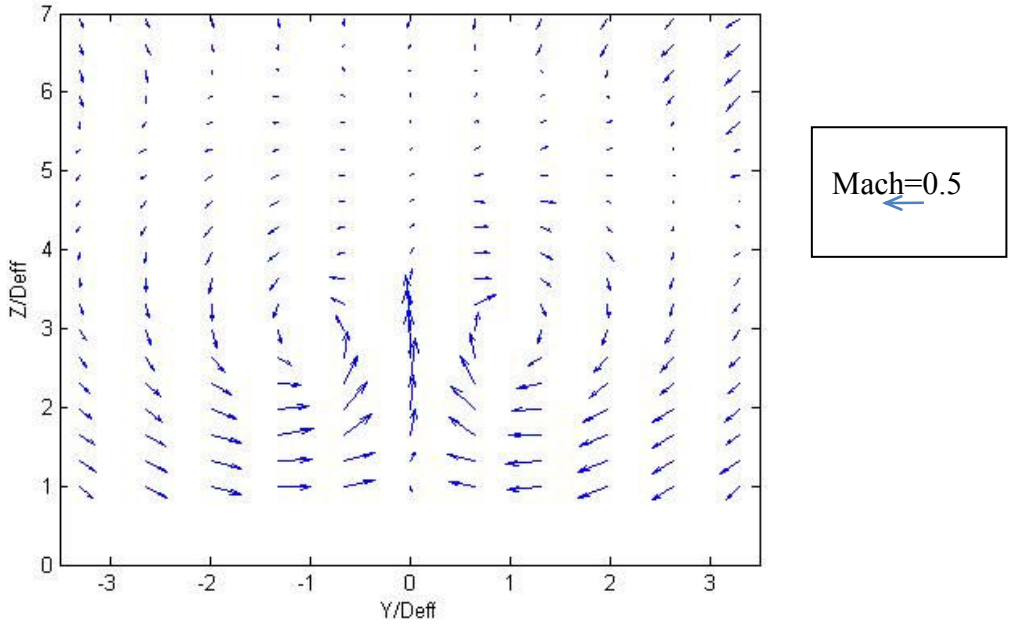

C)

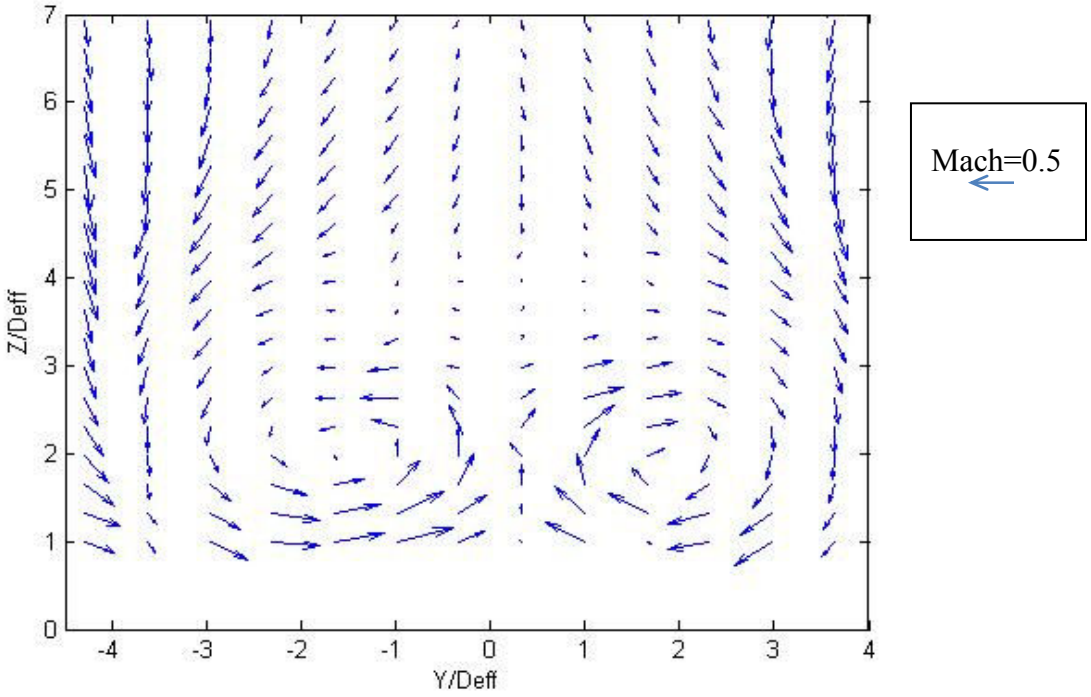

Figure 18. continued

Two measurements are used to quantitatively analyze the flow. $\mathbb{V}_z$ is the average height of the vortex centers, and $\mathbb{V}_y$ is the horizontal spacing between the vortices, both scaled in terms of d_{eff}. The uncertainty in these measurements is $\pm 0.1\, d_{eff}$. These quantities are tabulated in Table 3 below:

Table 3. Global parameters of vortices deduced from transverse Mach number data

Case	No Shock			Shock Upstream		Shock Downstream	
Injectant	Air	CH4	CO2	Air	CH4	Air	CH4
$\mathbb{V}_y\,(d_{eff})$	2.0	1.9	3.6	1.8	1.7	1.7	1.6
$\mathbb{V}_z\,(d_{eff})$	3.1	3.0	2.0	2.8	2.7	2.1	2.0

Being downstream of the shock reflection caused both the vortex height and spacing to decrease, indicating a decrease in plume size caused by the higher pressure downstream of the shock system. The shock reflecting downstream of the injector causes an additional reduction in the vortex height while only slightly reducing the spacing between the vortices, indicating a reduction in plume penetration but not size.

The vortex dimensions of air injection were slightly greater, than the lower molecular weight methane although generally within the margin of error. The carbon dioxide injection case again does not seem to fit into a clear pattern. The vortex centers for the CO_2 injection are much lower than those of either air or methane, while they are much more widely spaced. The wider spacing of the vortices means that the interaction between them will be reduced. The closer proximity of the vorticees to the wall seems to support the conclusion that the CO_2 plume core is lower than that of the other injectants, and possibly not as well mixed. Further analysis of this difference would be speculative without the availability of more data.

Comparable data from Maddalena's[17] studies included only a partial survey of the no-shock case, for which a $\mathbb{V}_z\,(d_{eff})$ of approximately 2.0 was estimated. This would seem to indicate significantly lower penetration. This would support the trend of increased penetration with increasing molecular mass that is observed between the methane and air cases.

A)

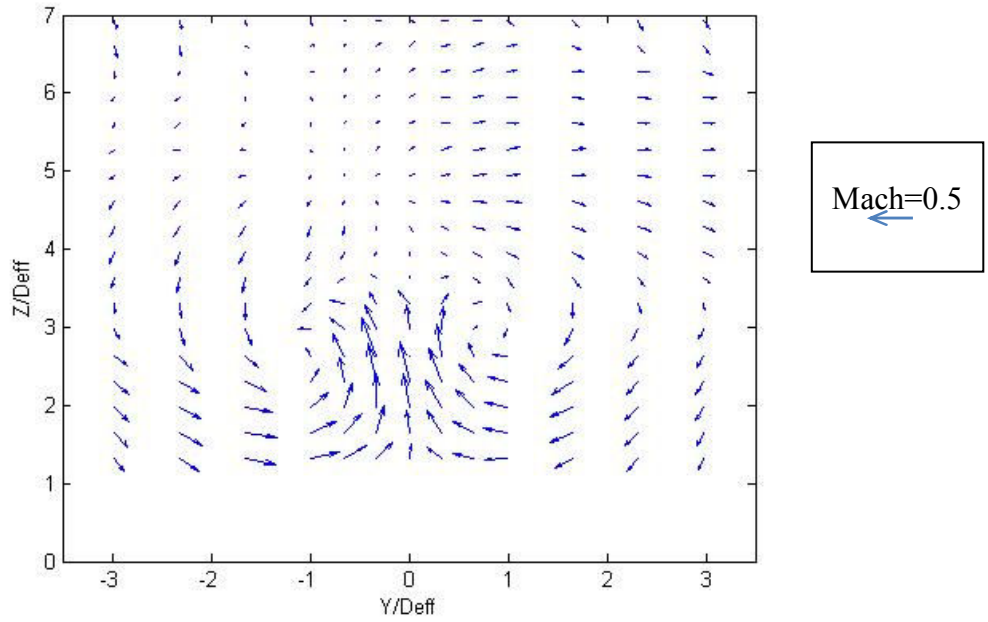

B)

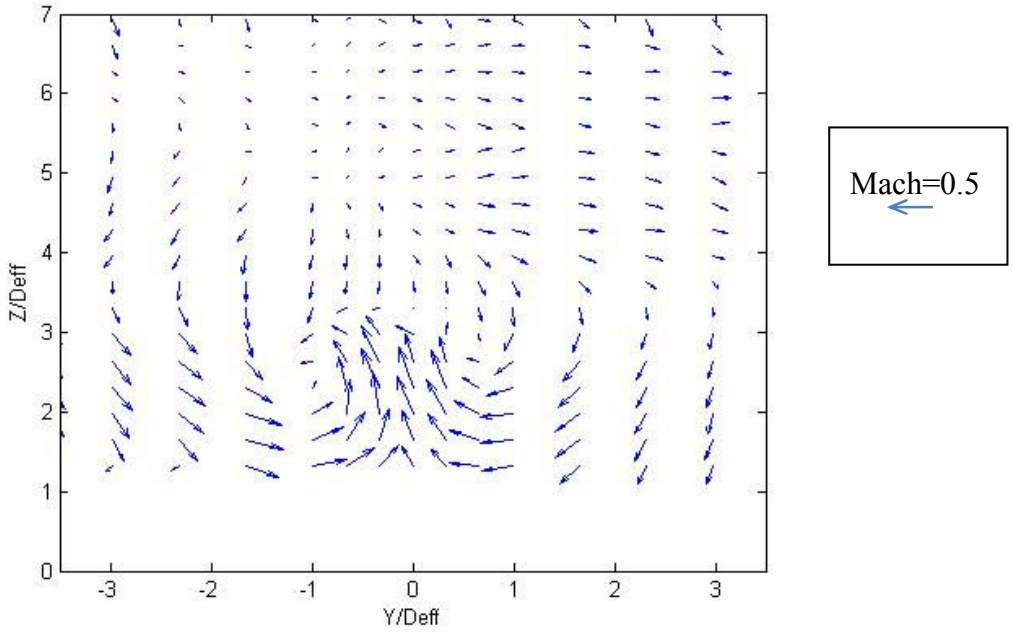

Figure 19. Transverse Mach number components for injection with shock impinging upstream of injector, A) air into air B) methane into air

A)

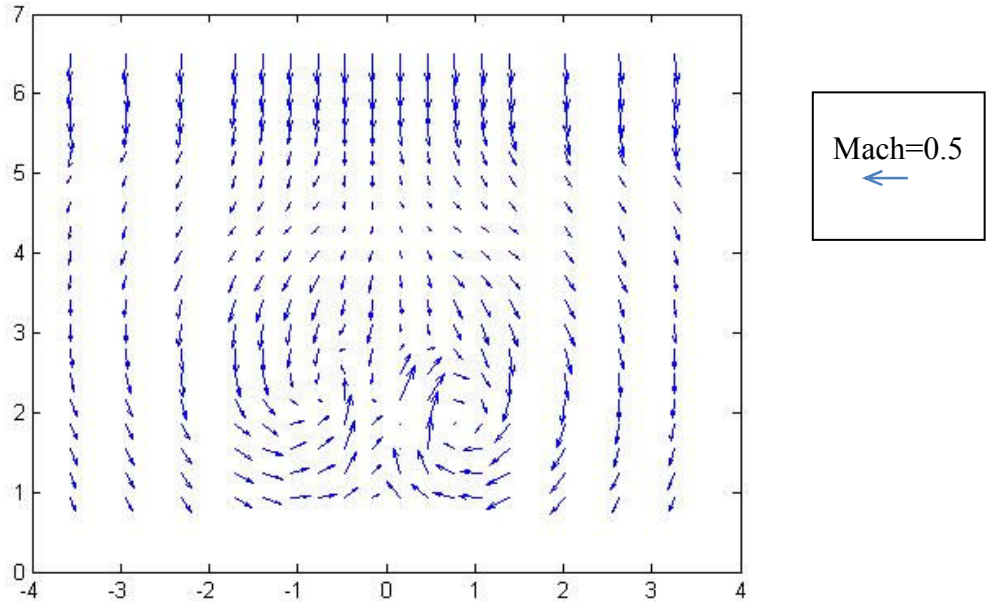

B)

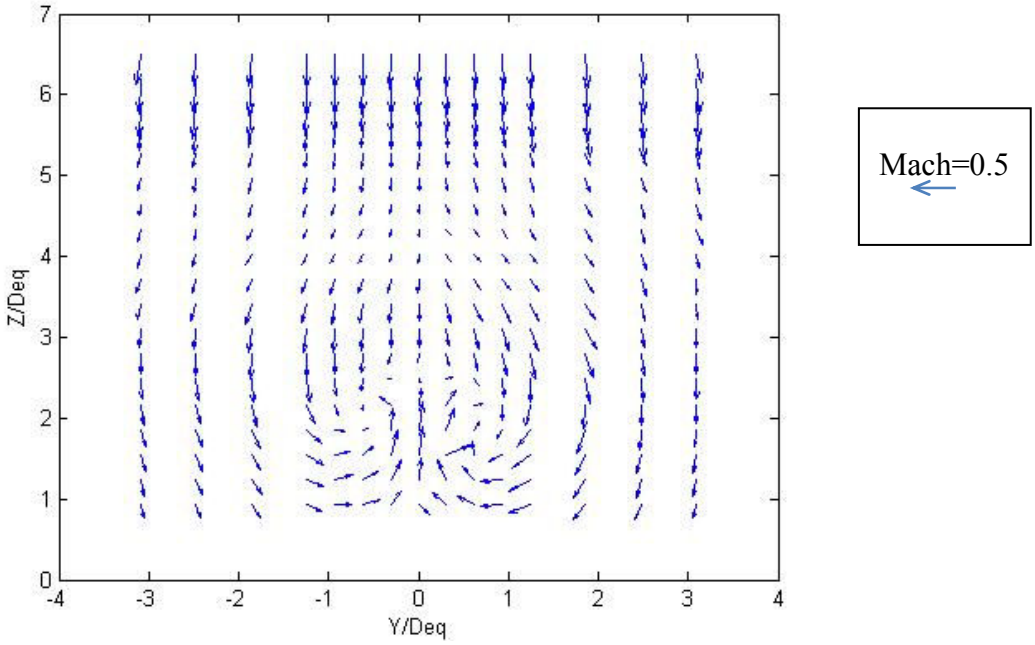

Figure 20. Transverse Mach number components for injection with shock impinging downstream of injector, A) air into air B) methane into air

D. MASS FRACTION CONTOURS

Mass fraction data obtained from the concentration probe for methane injection is given in the form of contour plots in Figure 21. The uncertainty in this data is ± 0.03 The CVP is evidenced by the double plume core that is formed. The plume core height is quantified as the vertical location of the maximum mass fraction $(\alpha_{max}), z^+$. The plume cores form at about 80% of the height of the vortex centers as determined from the methane Mach number contours. This is due to the fact that the CVP rise as the jet flows downstream and the concentration probe samples further upstream than the five-hole probe (13.9 vs. 17.2 d_{eff}). The plume width, $y^{\pm}$, is the width of concentrations above the methane/air stoichiometric value of 6.16%. These values are given in Table 4 below. Clearly, a shock impinging near the injection station increases mixing, whether it impinges upstream or downstream. The increase is larger for the downstream impingement. Maddalena[17], also found enhanced mixing for shock impingement downstream of helium injection.

The plume core is lower for the upstream shock impingement case than for the no-shock case, indicating that the plume does not penetrate as far due to the higher pressure behind the shock. For the case of shock impingement downstream of the injector, the plume core is lower than the upstream shock impingement case, showing that the plume is influenced by the strong pressure gradient produced by the shock.

A)

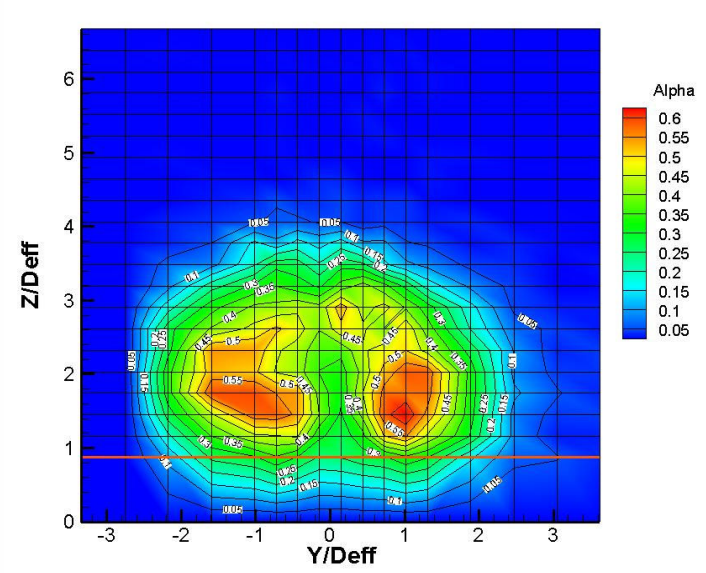

Figure 21. Mass fraction contours, A) undisturbed flow, B) shock impinging upstream of injector and C) shock impinging downstream of injector (Data below the red line is extrapolated)

B)

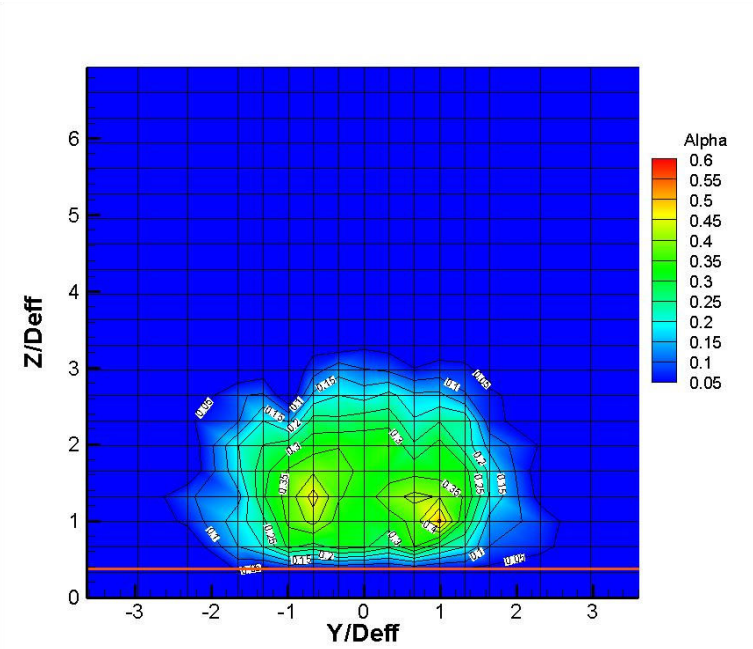

C)

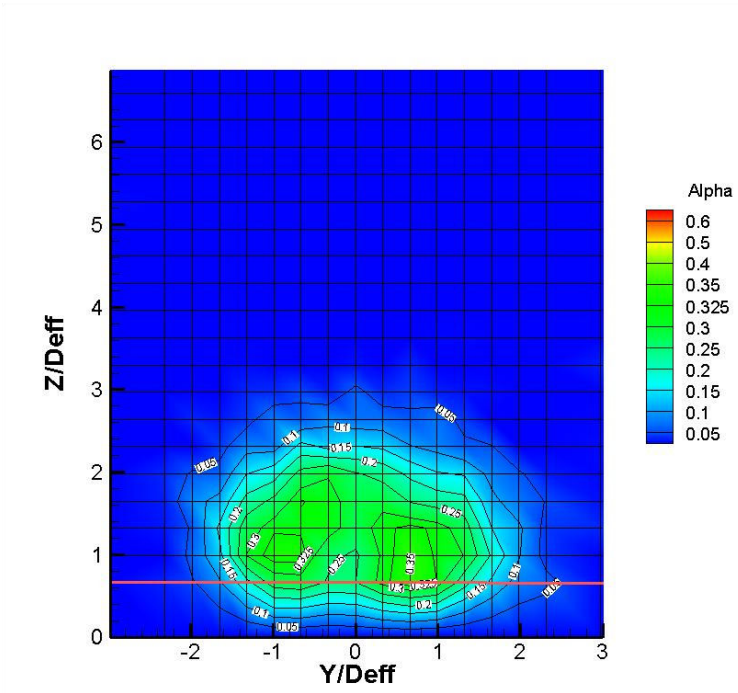

Figure 21. continued

The same effect was observed by Maddalena[17], performed concentration surveys with helium injection, both into undisturbed flow and with downstream shock impingement. His data appears to show the same trend of plume compression by the shock, although to a lesser degree. In particular his shock impingement case seems to show less vertical compression of the plume.

Table 4. Global parameters deduced from concentration contour plots

	No Shock	Shock Upstream	Shock Downstream
$y^{\pm}\left(d_{eff}\right)$	4.65	4.62	4.29
$z^{+}\left(d_{eff}\right)$	1.45	1.32	0.99
α_{max}	0.64	0.47	0.35

V. CONCLUSIONS

A study has been performed on the effects of injectant molecular weight on injection of a transverse jet in three cases: 1) an undisturbed Mach 4 free stream, 2) the same free stream with the addition of a shock wave impinging on the wall 4.5 d_{eff} upstream of the injector center, and finally 3) with a shock impinging 2.5d_{eff} downstream of the injector center. The three cases were also compared to one another. The three injectants used were air (W=28.97) methane (W=16.04) and carbon dioxide (W=44.01). Data from previous studies of helium injection (W=4.00) were used for reference. The momentum flux ratio and free stream conditions were held constant in all cases.

Three types of measurements were taken. A miniature five-hole probe was used to collect Mach number and flow angle data, which are presented as Mach number contours and Mach component plots. The Mach number contours were parameterized by the maximum height of the Mach 2.4 contour and the Mach component plots were parameterized by the height,$\mathbb{V}_z$, and spacing, $\mathbb{V}_y$, of the centers of the counter rotating vortex pair. A vacuum pump aspirated concentration probe was used to collect species concentration data, which was presented as contour plots. This data was parameterized by maximum concentration,α_{max}, height of maximum concentration, z^{+}, and plume width, $y^{\pm}$.

First, higher molecular weight injectant seems to increase penetration in general. In the undisturbed free stream case the centroid height of the Mach number defect, $\bar{z}_{M_*}$, was 3.52 d_{eff} for carbon dioxide injection, 2.64 for air injection and only 2.51 d_{eff} for methane injection. The CVP center height, $\mathbb{V}_z$, was 3.1 d_{eff} for air and 3.0 for methane. The case of the carbon dioxide injection was more complex. $\mathbb{V}_z$ was only 2.0 d_{eff}. The Mach number contour and the schlieren photograph of this case showed that the bow shock was stronger than in the air injection case. A carbon dioxide injection survey was done only for the undisturbed flow case.

In the case with the shock upstream of the injector Injection of air the $\bar{z}_{M_*}$ was 2.51 vs. 2.17 d_{eff} for methane. The CVP height was 2.8 vs. 2.7d_{eff}. For the case of shock impinging downstream of the injector $\bar{z}_{M_*}$ was 1.75 vs. 1.68 d_{eff} and $\mathbb{V}_z$ was 2.1 vs. 2.0.

Although the carbon dioxide case warrants additional examination in the future, the general trend seems to agree with the observations made by Ben-Yakar, Mungal and Hanson[24] who found that increasing molecular weight increased penetration due to its effect on periodic vortex production.

Increasing molecular weight increased the width of the CVP. In the undisturbed free stream case the lateral CVP spacing $\mathbb{V}_y$ increased from 1.9 d_{eff} with methane injection to 2.0 d_{eff} with air injection and 3.6 d_{eff} with carbon dioxide injection. In both shock impingement cases $\mathbb{V}_y$ is 0.1 d_{eff} greater for air injection than the lighter methane.

The addition of shock waves impinging before, and especially shortly after the injection jet significantly reduces penetration. The maximum concentration height z^+ was 1.45 d_{eff} for methane injection in an undisturbed free stream, 1.32 d_{eff} for upstream shock impingement and only 0.99 d_{eff} for downstream shock impingement. Reviewing the Mach data listed previously supports this as well. This is due to the increased flow pressure encountered by the jet and, with the jet impinging downstream of the injector, the turning of the flow towards the wall.

The interaction of a shock and an emerging jet increases mixing. As the jet mixes, the maximum concentration of injectant goes down, so maximum mass fraction, α_{max}, is used as a measure of the mixing rate. α_{max} for injection into an undisturbed free stream was 0.64. For shock impingement upstream α_{max} was 0.47. With the shock impinging downstream of the jet the maximum concentration was 0.35. Both of the shock interaction cases are affected by the addition of viscous effects of the reflection of the shock through the boundary layer. Additional vorticity generated here can explain increased mixing. That greater turbulence is present is supported by the fact that the CVP in the Mach contour plots is not as clearly developed for the shock interaction cases as in the undisturbed cases. In addition, the shock impinging downstream which the jet must pass directly through creates baroclinic torque which enhances mixing additionally.

Future work is needed in this area in order to better understand the effects of injectant molecular weight have on different mixing techniques. Not all injectants will necessarily respond to attempts at mixing enhancement in the same way, and these effects are little understood. This is a very relevant problem because the potential fuels for use in scramjet vehicles vary widely in properties including molecular weight and future designers of scramjet combustors must know what if any interaction the type of fuel used will have on what mixing enhancement techniques will be effective. Future studies could involve examinations of changing injectant weight on different mixing enhancement methods to determine how molecular weight affects their suitability.

In the near term, more analysis of the CO_2 injection case would be a useful next step. A more detailed examination is needed to fully understand why the results do not appear to be a smooth extrapolation of the other data available. More powerful visualizations, either optical or computational could determine if there is some change in the flow features that explains the change in pattern detected by this study. A survey of the concentration field could reveal if the plume is in fact closer to the wall as hypothesized here.

A better understanding of these complex high speed flow physics will lead to a more robust predictive ability of scramjet combustor performance, and that is a critical step in improving our ability to design and construct the scramjet powered vehicles of the future.

REFERENCES

[1]E.T. Curran, "Scramjet Engines: The First Forty Years" Journal of Propulsion and Power vol. 17, no 6, November-December 2001

[2] R. S. Fry, "A century of ramjet propulsion technology evolution," Journal of Propulsionand Power, vol. 20, no. 1, pp. 27–58, 2004.

[3]McClinton, C.R., " The effect of Injection Angle on the interaction Between Sonic Secondary Jets and a Supersonic Freestream," NASA TND-6669, February 1972.

[4]Rogers, R.C., "A study of the Mixing of Hydrogen Injected Nomal to a Supersonic Airstream," NASA TN L-7386, Langley Research Center, March 1971.

[5]Povinelli, L.A., and Ehlers, R.C.," Swirling Base Injection for Supersonic Combustion Ramjets," AIAA Journal, Vol. 10 No. 9, pp. 1243-1244, September, 1972.

[6]Hartfield, R.J., Hollo, S.D., and McDaniel, J.C.,"Experimental Investigations of a Supersonic Swept Ramp Injector using Laser Induced Iodine Fluorescence,"Journal of Propulsion and Power, Vol.10 No.1,1994, pp. 129-135, January-February.

[7]Fuller, E.J., Mays, R.B., Thomas, R.H., and Schetz, J.A.," Mixing Studies of Helium in Air at Mach 6," AIAA Paper 91-2268, June, 1991.

[8]Barber, M.J., Roe, L.A., and Schetz, J.A., "Simulated Fuel Injection through a Wedge Shaped Orifice in a supersonic Flow," AIAA Paper 95-2559, July 1995.

[9]Kraus, D. K., and Cutler, A. D., "Mixing of Swirling Jets in a Supersonic Duct Flow, " Journal of Propulsion and Power, Vol. 12, No. 1, 1996, pp. 170-177, January-February.

[10]Cutler, A.D., and Johnson C. H., "The Use of swirling Jet Pairs to Provide Rapid Fuel Penetration in Scramjet Combustors," AIAA Paper 95-0099.

[11]Mao, M. Riggins, D. W., and Mc Clinton C.R., "Numerical Simulation of Transverse Fuel Injection, "NASP CR 1089, May 1990.

[12]Cox, S.K., Fuller, R.P., and Schetz, J.A., "Vortical Interactions Generated by a Injector Array to Enhance Mixing in a Supersonic Flow," AIAA Paper 94-0708, January 1994.

[13]Doerner S.E., and Cutler A.D., "Effects of Jet Swirl on Mixing of a Light Gas Jet in a Supersonic Airstream", NASA/CR-1999-209842, December 1999

[14]Schetz J.A., Cox-Stouffer S., and Fuller R., "Integrated CFD and Experimental Studies of Complex Injectors in Supersonic Flows", AIAA 98-2780, June 1998

[15]Fuller R.P., Wu P.K., Nejad A.S., and Schetz J.A., "Comparison of Physical and Aerodynamic Ramps as Fuel Injectors in Supersonic Flow", Journal of Propulsion and Power, Vol. 14, No. 2, March-April 1998

[16]Tomioka, S., Jacobsen, L.S., and Schetz, J.A., " Interaction Between a Supersonic Airstream and a Sonic Jet Injected throught a Diamond-shaped Orifice," AIAA Paper 2000-0088, January 2000.

[17]Maddalena, L. "Investigations of Injectors for Scramjet Engines" PhD. Dissertation, Virginia Tech, July 2007

[18]A. Ben-Yakar, M. G. Mungal, and R. K. Hanson." Transverse jets in supersonic crossflow, Part 2: The Effect of Compressibility, Velocity Ratio and Density Ratio". Physics of Fluids, 2005.

[19]Schetz, J.A., *Injection and Mixing in a Turbulent Flow*, AIAA, New York, New York, 1980.

[20]Schetz, J.A., Thomas, R.H., and Billig, F.S., "Mixing of Transverse Jets and Wall Jets in Supersonic Flow," IUTAM Symposium on Separated Flows and Jets, Novosibirsk, July 1990.

[21]Yuan, L.L and Ferzieger, H. "Large Eddy Simulation of a Round Jet in Crossflow", Journal of Fluid Mechanics, 379, 71-104

[22]R. Srinivasan and R. D. W. Bowersox, "Simulation of transverse gaseous injection through a diamond port into a mach 5.0 freestream," in 43rd AIAA Aerospace SciencesMeeting and Exhibit, 10 - 13 January, Reno, Nevada, 2005.

[23]L. Cortelezzi and A. Karagozian, "On the formation of the counter-rotating vortex pair in transverse jets," Journal of Fluid Mechanics, vol. 446, pp. 347–373, 2001.

[24]A. Ben-Yakar, M. Mungal, and R. Hanson, "Time evolution and mixing characteristics of hydrogen and ethylene transverse jets in supersonic crossflows," Phys. Fluids,vol. 18, p. 026101, 2006.

[25]J.A. Schetz and F.S. Billig, "Penetration of Gaseous Jets Injected Into a Supersonic Stream," AIAA Journal of Spacecraft Vol. 3, No. 11, AIAA 28721-239

[26]R.C. Orth and J.A. Funk, "An Experimental and Comparative Study of Jet Penetration in Supersonic Flow" AIAA Paper 1967-225

[27]D. Papamoschou and DG. Hubbard, "Visual Observations of Supersonic Transverse Jets" Experiments in Fluids, Vol. 14 No. 6, pg 468-476

[28]M.R. Gruber, A.S. Nejad, T.H. Chen, and J.C. Dutton "Mixing and Penetration Studies of Sonic Jets in a Mach 2 Freestream" Journal of Propulsion and Power, Vol. 11 No. 2 March-April 1995

[29]K. Hirano, A. Matsuo, T. Kouchi, M. Izumikawa, and S. Tomioka, "New injectorgeometry for penetration enhancement of perpendicular jet into supersonic flow," in 43rd Joint Propulsion Conference and Exhibit, 8 - 11 July, Cincinnati, OH, 2007.

[30]R.J. Ungewitter, J.D. Ott and S.M. Dash "Advanved Modeling Methods for Hypersonic Scramjet Evaluation:42nd AIAA/ASME/SAE/ASEE Joint Propulsion Conference and Exhibit 9-12 July 2006, Sacramento, CA

[31]W. F. Ng, F. T. Kwok and T.A. Ninnemann, " A Concentration Probe for the Study of Mixing in Supersonic Shear Flows," AIAA paper 89-2459, July 1989.

[32]Centolanzi, F.J. "Characteristics of a 40 Cone for Measuring Mach Number, Total pressure, and Flow Angles at Supersonic Speed," NACA TN-3967, May 1957

[33]Swalley, F.E. "Measurement of Flow Angularity at Supersonic and Hypersonic Speeds with the use of a conical probe",NACA TN D-959, September 1961.